Dynamical Phase Transition in a Driven Disordered Vortex Lattice

Seungoh Ryu,[1] M. Hellerqvist,[2] S. Doniach,[2] A. Kapitulnik,[2] and D. Stroud[1]
[1]*Department of Physics, The Ohio State University, Columbus, Ohio 43210*
[2]*Department of Applied Physics, Stanford University, Stanford, California 94305*
(Received 18 June 1996)

Using Langevin dynamics, we have investigated the dynamics of vortices in a disordered two-dimensional superconductor subjected to a uniform driving current. The results provide direct numerical evidence for a dynamical phase transition between a plastic flow regime and a moving "hexatic glass." The simulated current-voltage characteristics are in excellent agreement with recent transport measurements on amorphous $Mo_{77}Ge_{23}$ thin film superconductors. [S0031-9007(96)01833-9]

PACS numbers: 74.60.Ge, 05.70.Fh, 64.60.Cn, 74.60.Jg

While the effects of disorder on the *static* Abrikosov lattice have been widely discussed [1,2], the *driven* disordered lattice has been much less studied, despite its obvious relevance to typical transport measurements. Schmid and Hauger [3] analyzed interactions between a pinning potential and the elastically deformed moving lattice. Several groups [4,5] have numerically demonstrated the importance of plastic deformation and associated dislocations in driven two-dimensional (2D) lattices. Recently, hysteretic, filamentary flow has been found numerically in the plastically deformed regime [6].

An actual *dynamic phase transition* between the plastically deformed phase and a moving lattice for the vortex lines was first proposed and numerically demonstrated in 2D by Koshelev and Vinokur [7]. Their idea is that the random "pinning noise" diminishes with increasing vortex velocity, allowing a high-velocity reordering. Because of the disorder, the moving lattice is argued to be a novel "moving glass" phase with a finite transverse critical current [8]. Similar dynamical ordering phenomena may affect Wigner electron crystals [9], vortex lattices in Josephson arrays [10], magnetic bubble arrays [11], and charge-density-wave systems [12,13].

Experimentally, a dynamical transition into a moving lattice phase has been suggested by transport measurements [14], neutron diffraction [15] on flux lines in 2H-$NbSe_2$, and the current-voltage (I-V) characteristics in the 2D amorphous superconductor $Mo_{77}Ge_{23}$ [16]. The latter displays maxima in dV/dI [16], suggesting a dynamical ordering transition.

This Letter reports numerical studies of a model 2D vortex system which show evidence for *three distinct dynamical phases*. The evidence comes from calculations of both the I-V's and the translational and hexatic order parameters. We also obtain a finite transverse critical current in the high-drive ordered phase, and a striking crossing of all the dV/dI curves for different temperatures at a single point ($I_{\rm cr}$, $V_{\rm cr}$), in excellent agreement with experiment [16].

We consider N_v two-dimensional vortices located at $\mathbf{r}_i$ in a thin superconducting layer of thickness d, bulk penetration depth $\lambda(T) = \lambda(0)/\sqrt{1 - T/T_c}$, and fixed vortex density $n_B \equiv 1/a_B^2 \equiv B/\phi_0$, where $\phi_0 = hc/2e$. The classical Hamiltonian for the system is taken as

$$\mathcal{H} = \left[\sum_{i>j} U\left(\frac{d|\mathbf{r}_i - \mathbf{r}_j|}{\lambda^2(T)}\right) + \sum_i V(\mathbf{r}_i)\right]. \quad (1)$$

The repulsive intervortex interaction is $U(x) = [d\phi_0^2/8\pi^2\lambda(T)^2]K_0^*(x)$, where $K_0^*(x)$ is a summation of the modified Bessel function $K_0(x)$ over image vortices under periodic boundary conditions in the x-y plane [17,18]. The disorder potential $V(r)$ is taken as N_p potential wells of uniform depth $U_p(T,B) = \alpha_p d\phi_0^2/[64\pi^2\lambda^2(T)]$ and radius r_p. To carry out the calculation for a given random pin configuration, we first anneal the system from $T \sim T_c$ down to $T = 100$ mK, in steps of $\triangle T = 200$ mK, using the Metropolis algorithm [19]. At each temperature T of interest, we take a snapshot $\{\mathbf{r}_i\}^0_{T,J=0}$ of the vortex configuration during the annealing process, to be used as the initial dynamical configuration.

The vortex dynamics are obtained from the overdamped equation

$$\eta\dot{\mathbf{r}}_i(t) = \mathbf{f}_i^T(t) + \mathbf{f}_i^U(t) + \frac{\phi_0}{c}\mathbf{J}\times\hat{z} + \mathbf{f}^P(\mathbf{r}_i). \quad (2)$$

The first term on the right-hand side is the Brownian force due to Gaussian thermal noise [7]. The remaining terms are the forces per unit vortex length due, respectively, to the other vortices, the applied current, and a smoothed version of the random pinning potential of Eq. (1), as described in detail in [18]. In actual runs, we used the $Mo_{77}Ge_{23}$ [16] parameters $\lambda(0) = 7700$ Å, Ginzburg-Landau parameter $\kappa = 140$, $d = 60$ Å (and hence $\lambda^2/d = 98.8$ μm), $T_c = 5.63$ K. Our bounding box containing 256 vortices for $B = 0.5$ kG has an edge $L_x \sim 3.2$ μm, and we include up to 200×230 image boxes within a circle, comprising a total linear dimension $\tilde{L} \sim 6.5\lambda^2(0)/d$. We use a time step of $0.1-1 \times t_0$ where $t_0 = \eta\lambda^2\pi^2/16B\phi_0$, an areal pin density $B_p/B = 4.0$, and we take $r_p = 2\xi_{ab}(0)$, $\alpha_p = 1$. We also introduce a current density scale J_p by $d\phi_0 J_p/c \equiv U_p(0)/r_p$. For our parameters, $J_p = 5.05 \times 10^5$ (A/cm^2), about 8% of the depairing critical current density. Typically we discard the first $5000t_0$ of time steps to assure achievement of a steady state.

 0031-9007/96/77(25)/5114(4)$10.00

To trace the disclination density $n_d(t)$ (i.e., sites with coordination number $\neq 6$), we perform Delaunay triangulation on $\{\mathbf{r}_i(t)\}_{T,J}$ every $10t_0$. We also measure (typically averaged over $\tau = 20\,000t_0$) the vortex density-density correlation function $G(\mathbf{r}) = \frac{1}{\tau}\int^{\tau} dt\langle\rho(\mathbf{r},t)\rho(\mathbf{0},t)\rangle$, its Fourier transform $S(\mathbf{q})$, and the hexatic order parameter Ψ_6 [20]. *I-V* characteristics are obtained from the center of mass drift velocity of the entire vortex ensemble, and the Josephson relation $\mathbf{E} = n_B\phi_0\mathbf{v}/c \times \hat{z}$.

With no pins, we find that the lattice has a first order melting transition at $T_m = 0.41T_c$, with a Lindemann number of 0.19, and a simultaneous vanishing of both translational and hexatic order. This T_m is reasonably close to the upper bound obtained from the dislocation unbinding picture: $k_BT_m = A_1(d\phi_0^2/128\sqrt{3}\,\pi^3\lambda^2(T_m))$, provided the renormalization constant $A_1 \approx 0.85$ [21]. With point pins, the vortices freeze into a disordered state with some residual hexatic order. An upper limit T_f^+ for the freezing temperature may be operationally defined as the point where the self-diffusion measure $\langle|\mathbf{r}_i(t) - \mathbf{r}_i(0)|^2\rangle$ converges to a t-independent value. We find that the $T_f^+ \sim 2.0$ K $\sim 0.87T_m$.

Figure 1 shows the simulated *I-V* characteristics at several temperatures. The results at the lowest temperature ($T/T_m = 0.043$) most clearly show that there are *three distinct regimes* [22]. (i) At low driving currents ($J/J_p < 0.2$), the lattice is pinned and the voltage is generated mainly by *rearrangements of topological defects*, which produce a very slow and unsteady advance of the pinned lattice. At least over the simulation time ($\sim 50\,000t_0$), the quenched-in hexatic order stays robust; we may therefore call this regime a *pinned hexatic vortex glass* (PHVG). (ii) At moderate J ($0.2 < J/J_p < 1.2$), the *I-V*'s are strongly nonlinear. The hexatic order is progressively destroyed with increasing J. The nonlinearity originates from the nature of plastic deformations in this regime, with highly filamentary vortex trajectories (cf. insets of Fig. 2). Deep into this state, $\Psi_6 \approx 0$ and the system is a *plastic flow vortex liquid* (PFVL). (iii) At high J, the lattice heals incompletely, and hexatic order is dramatically enhanced ($\Psi_6 \sim 0.6$) over the static phase (i) ($\Psi_6 \sim 0.03$). Translational order is still disrupted by a comoving pattern of neutral disclination pairs. Both $g(r)$ and $S(k)$ display a strong anisotropy. We may thus call this state a *moving hexatic vortex glass* (MHVG).

The simulated dV/dI curves shown in Figs. 2 and 3 reproduce most of the essential experimental features [16]. At the lowest T, Fig. 2 shows that the peak in the calculated dV/dI coincides with the dip in Ψ_6. At higher temperatures the peak broadens and merges with the region where Ψ_6 again starts to increase. In the simulations, the dynamic freezing transition (operationally defined as

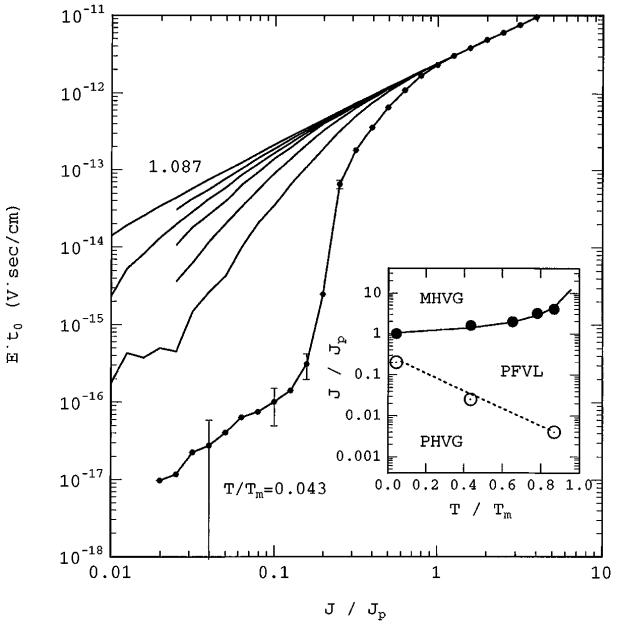

FIG. 1. Simulated *I-V* characteristics for $T/T_m = 0.043$, 0.43, 0.65, 0.78, 0.87, 0.96, and 1.087. Error bars on selected points are rms deviation of measurements taken over ten different time windows over a total of $200\,000t_0$ for a given realization of disorder. We assume the system is sufficiently large that the disorder potential is self-averaging. Inset: *J-T* phase diagram constructed from the *I-V* results and analyses of Ψ_6 (Fig. 2). The solid line $[J/J_p = 1.2 + 1.2/(1 - T/T_m)]$ and the broken lines are guides to the eye. Acronyms defined in the text.

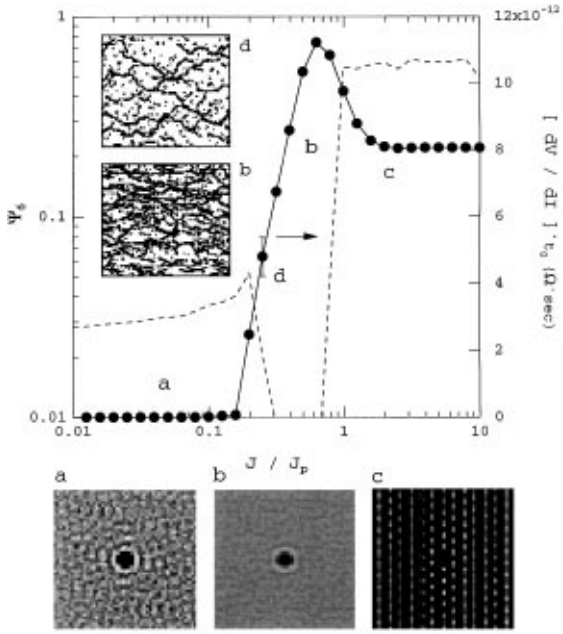

FIG. 2. Hexatic order parameter Ψ_6 (broken line) and differential resistance dV/dI for $T/T_m = 0.043$. Error bars in Fig. 1 are carried over for dV/dI here, but only one is visible in this scale. Inset: vortex trajectories at points b and d in the plastic regime taken over $1000t_0$. The dots represents those pinned vortices which remained static over this interval. Lower panel shows the time averaged $g(r)$ for J/J_p: 0.04, 0.4, and 1.98; they are marked a (PHVG), b (PFVL), and c (MHVG).

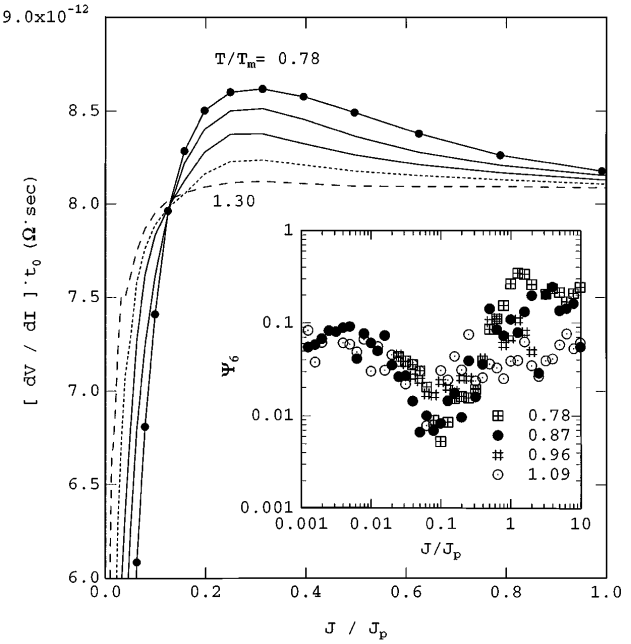

FIG. 3. Simulated dV/dI for $T/T_m = 0.78$, 0.87, 0.96, 1.087, and 1.30 near melting. Inset shows Ψ_6. The crossing of all the dV/dI curves near $J/J_p \sim 0.12$ coincides with the dip in Ψ_6.

the sharp increase of Ψ_6 at $J \sim 0.8J_p$) falls on the right-hand shoulder of the peak. In the experiment [16], the peak was interpreted as representing the increase in lattice correlation, since it follows remarkably well the Koshelev-Vinokur prediction [7]. We therefore conclude that the peak in dV/dI marks the point where both orientational and positional lattice correlations *start to increase*. In the plastic regime [left shoulder of the peak], the density and tortuosity of the calculated vortex trajectories are very sensitive to both J and T (presumably via the T-dependent effective shear modulus of the vortex lattice). Qualitatively, the current paths resemble percolation paths just above the percolation threshold. We suggest that the current travels along an "infinite connected cluster" of open paths. These paths occupy an area which increases with increasing J, perhaps as a power law in $(J - J_0)$, J_0 being the current density where the infinite cluster first forms.

As $T \to T_m$, the dV/dI isotherms all tend to cross at a $J_{\rm cr} \sim 0.12J_p$, strikingly reproducing a prominent experimental feature [16]. The pinned fraction of the vortices also starts a sharp decrease at this same value of J/J_p. Furthermore, as the inset of Fig. 3 shows, this crossing coincides with the minimum in Ψ_6. For $J < J_{\rm cr}$, we found that the vortex flow is composed of two components: unpinned individual vortices in the flux-flow state and pinned vortex islands with local hexatic order. The latter contribute to the flow through intermittent motion. As J increases toward $J_{\rm cr}$, the size of the pinned islands shrinks and, consequently, the moving vortex trajectories become less tortuous. We speculate that for each T, $J_{\rm cr}(T)$ is the current density where the dV/dI for the pinned and unpinned contributions become comparable.

Finally, we consider the MHVG. In all our simulations, the moving healed lattice carries along bound disclination pairs ranging in density from 0.05 at $T/T_m = 0.043$ to 0.4 at $T/T_m = 0.96$. In the rest frame of the average velocity v, the lattice has local triangular order, but long-range translational order is disrupted by the disclination pairs (cf. Fig. 4).

This behavior suggests that the MHVG/PFVL is really dynamical freezing, as suggested by [7]. To confirm this interpretation, we estimate the effective "disorder temperature" T_d. Viewed in the moving frame, the pins provide a random time-dependent potential which corresponds to an effective T_d. For the present pinning potential, a simple analysis, including the vector nature of the forces, yields $k_B T_d = 0.56U_p^2/va_p d\eta$. Here $a_p = 1/\sqrt{n_p}$, where n_p is the number density of pins. For our system, at zero temperature, $U_p = 7.5 \times 10^{-15}$ erg, and $a_p = 1.02 \times 10^{-5}$ cm. Using $E = Bv/c$, where E is the electric field, we finally obtain $T_d(\mathrm{K}) \approx 6.6 \times 10^{-12}/Et_0$. For low temperatures ($T/T_m \approx 0.043$), the PHVG/MHVG melting transition occurs near $Et_0 \approx 3 \times 10^{-12}$ V sec/cm, or equivalently $T_d \approx 2.2$ K, in excellent agreement with the simulated pin-free melting temperature.

In the MHVG phase, the lattice principal axis is *not always parallel* to the driven direction. The degree of misalignment in the annealed lattice correlates with the angle between the drift and driving directions [3], suggesting the

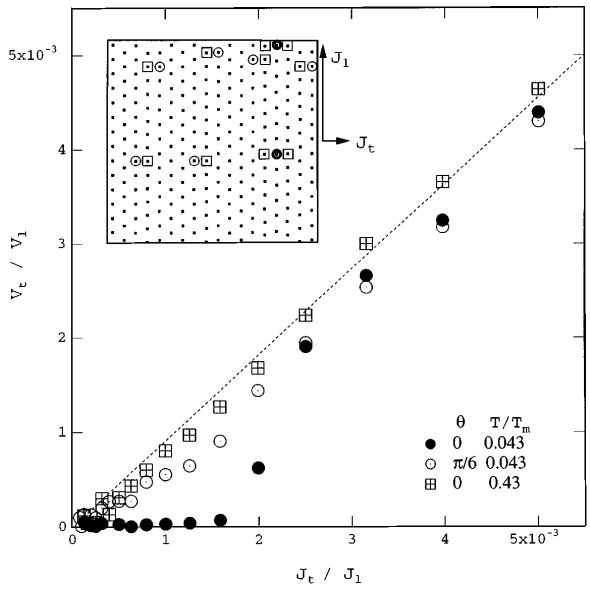

FIG. 4. Transverse voltage induced by a transverse force $\hat{z} \times J_t \parallel \hat{\mathbf{x}}$. J_t is turned on after a steady state is reached under the dominant force $\hat{z} \times J_\ell \parallel \hat{\mathbf{y}}$. Both $T/T_m = 0.043$ (solid) and 0.43 (broken) are shown. Inset: snapshot of vortices (points) for $\theta = 0, T/T_m = 0.043$. A pattern of disclinations with coordination numbers $z = 8$ (filled circle), 7 (open circle), and 5 (square) is also shown.

possibility of an anomalous Hall effect. This misalignment may occur because the lattice in MHVG is biased toward a direction which is frozen in during the $J = 0$ annealing, and thereafter frustrated from rotating parallel to the applied drive. To confirm this, we repeated with random initial configurations instead of an annealed state. The lattice then oriented its principal axis parallel to the driven direction, but the resulting state was *higher in total energy than in the annealed case, with about twice the number of disclinations.*

Finally, we note the nonzero *transverse critical current* J_{tc} in MHVG. To see this, the lattice is first set in motion along a prescribed direction $\hat{\ell}$ (of magnitude $J_\ell/J_p = 2.6$ in our simulations) for $20\,000t_0$. Then a small transverse current $0 < J_t/J_\ell < 0.01$ is turned on along $\hat{\mathbf{t}} = \hat{\ell} \times \hat{z}$, and the lattice transverse velocity v_t is measured over $10\,000t_0$. The results are shown in Fig. 4 for two angles θ between $\hat{\ell}$ and a local principal axis of the moving lattice: $\theta = 0$ and $\theta = \pi/6$. For $\theta = 0$ and $T/T_m = 0.043$, v_t drops abruptly at $J_t/J_\ell = 0.002$. For $\theta = \pi/6$, this drop is much less sharp. This transverse barrier disappears very rapidly with increasing T, as shown for $T/T_m = 0.43$, $\theta = 0$. A possible explanation for this behavior is suggested by the inset, which shows the quenched disclination patterns (open circle and squares) of the moving phase. Presumably, during transverse lattice motion, these quenched defects slip, possibly reducing J_{tc} below the predictions of elastic theory, which forbids such slippage. All these dynamic phases will probably manifest themselves more clearly in three dimensions. In BiSrCaCuO-type materials, observation by neutron diffraction [23] of a low-T field-induced disordering transition was interpreted as a topological phase transition from an ordered line lattice to a decoupled glass phase [24]. The glass phase has quasi-2D topological defects at low T, which may have I-V similar to those described here. Thus, by driving the vortices with a high J *at varying fields,* and carrying out both resistivity and Hall measurements, one may be able to probe the moving lattice phase and its lower critical dimension.

As this work was being completed, we became aware of work by Moon *et al.* on a similar model [25]. This work was supported by the Midwest Superconductivity Consortium through DOE Grant No. DE-FG02-90ER-45427 and NSF Grants No. DMR-9508419-A001 and No. DMR94-02131.

[1] A. I. Larkin, Sov. Phys. JETP **31**, 784 (1970); A. I. Larkin and Y. N. Ovchinnikov, *ibid.* **34**, 651 (1972).

[2] J.-P. Bouchaud *et al.*, Phys. Rev. B **46**, 14 686 (1992); T. Nattermann, Phys. Rev. Lett. **64**, 2454 (1990); T. Giamarchi and P. LeDoussal, *ibid.* **72**, 1530 (1994); T. Giamarchi and P. LeDoussal, Phys. Rev. B **52**, 1242 (1995); E. M. Chudnovsky, *ibid.* **40**, 11 355 (1989).

[3] A. Schmid and W. Hauger, J. Low Temp. Phys. **11**, 667 (1973).

[4] H. J. Jensen *et al.*, Phys. Rev. Lett. **60**, 1676 (1988).

[5] A.-C. Shi and A. J. Berlinsky, Phys. Rev. Lett. **67**, 1926 (1991).

[6] N. Grønbech-Jensen *et al.*, Phys. Rev. Lett. **76**, 2985 (1996).

[7] A. E. Koshelev and V. M. Vinokur, Phys. Rev. Lett. **73**, 3580 (1994).

[8] T. Giamarchi and P. L. Doussal, Phys. Rev. Lett. **76**, 3408 (1996).

[9] M.-C. Cha and H. A. Fertig, Phys. Rev. B **50**, 14 368 (1994).

[10] F. Falo *et al.*, Phys. Rev. B **41**, 10 983 (1990); D. Dominguez *et al.*, Phys. Rev. Lett. **72**, 3096 (1994).

[11] R. Seshadri and R. M. Westervelt, Phys. Rev. B **46**, 5142 (1992); **46**, 5150 (1992).

[12] D. Fisher, Phys. Rev. B **31**, 1396 (1985); A. Middleton, Phys. Rev. Lett. **68**, 670 (1992).

[13] L. Balents and M. P. A. Fisher, Phys. Rev. Lett. **75**, 4270 (1995).

[14] S. Bhattacharya and M. J. Higgins, Phys. Rev. Lett. **70**, 2617 (1993); Phys. Rev. B **49**, 10 005 (1994); A. C. Marley *et al.*, Phys. Rev. Lett. **74**, 3029 (1995).

[15] U. Yaron *et al.*, Nature (London) **376**, 753 (1995).

[16] M. C. Hellerqvist *et al.*, Phys. Rev. Lett. **76**, 4022 (1996).

[17] Our choice of $K_0(rd/\lambda^2)$ instead of $\frac{2}{\pi}[H_0(r/\Lambda) - Y_0(r/\Lambda)]$ [6] introduces an effective cutoff of λ^2/d. But with our periodic boundary condition and $\lambda^2/dL \gg 1$, where L is the simulation cell edge, we have verified numerically that these forms differ by less than 0.1% with up to 200×230 images. All our results are obtained in the regime $\lambda^2/dL \gg 1$, suggesting that the experimental features [16] we discuss are dominated by physics at length scales smaller than λ^2/d.

[18] See Eqs. (9) and (10) in Seungoh Ryu and D. Stroud, Phys. Rev. B **54**, 1320 (1996).

[19] S. Ryu *et al.*, Phys. Rev. Lett. **68**, 710 (1992).

[20] After Delaunay triangulation, the local hexatic order parameter is evaluated from $\Psi_6 = |\frac{1}{N}\langle\sum_{i,j'}\frac{1}{c_i}\exp[i6\theta_{ij}]\rangle|$ where N is the total number of pancakes, c_i the vortex coordination number, and θ_{ij} is the bond angle between neighboring vortices relative to a fixed direction $\hat{x}$.

[21] D. J. Thouless, J. Phys. C **11**, L189 (1978); B. I. Halperin and D. R. Nelson, Phys. Rev. Lett. **41**, 121 (1978); A. P. Young, Phys. Rev. B **19**, 1855 (1979); B. A. Huberman and S. Doniach, Phys. Rev. Lett. **43**, 950 (1979); D. S. Fisher, Phys. Rev. B **22**, 1190 (1980). For reviews of computer simulations of 2D melting with various interactions, see K. J. Strandburg, Rev. Mod. Phys. **60**, 161 (1988); H. Kleinert, *Gauge Fields in Condensed Matter* (World Scientific, Singapore, 1989), Vol. II, Chap. 14.

[22] Representative movies showing this behavior can be found at http://www.physics.ohio-state.edu:80/~ryu/moge.html

[23] R. Cubitt *et al.*, Nature (London) **365**, 407 (1993).

[24] Seungoh Ryu *et al.*, Phys. Rev. Lett. **77**, 2300 (1996); M. J. P. Gingras and D. A. Huse, Phys. Rev. B **53**, 15 193 (1996).

[25] K. Moon *et al.* (to be published).